Superalloys 2020: Proceedings of the 14th International Symposium on Superalloys,
13-16 September, Virtual Event, The Minerals, Metals & Materials Series. Springer, Cham
https://doi.org/10.1007/978-3-030-51834-9_75

Measurement and Evaluation of Co-Existing Crack Propagation in Single Crystal Superalloys in Hot Corrosion Fatigue Environments

L. Brooking[1], C. Ferguson[1], J. Mason-Flucke[2], G. Gibson[2], J. Leggett[2], I. Palmer[1], J.R. Nicholls[3] and S. Gray[3*]

[1]Frazer-Nash Consultancy, 1 Lower Lamb St, Bristol, BS1 5UD, UK
[2]Rolls-Royce plc, PO Box 31, Derby, DE24 8BJ, UK
[3]SEPI, Cranfield University, Bedford, MK43 0AL, UK
[*]Corresponding author S.Gray@Cranfield.ac.uk

Keywords: SC Superalloys, Crack Growth, Potential Difference, Corrosive Environments, Stress Intensity

Abstract

Gas turbines blades are required to operate at high temperatures whilst being subjected to stress and corrosive environments. These demanding conditions have led to the need to better understand the interactions between corrosion and loading in order to improve lifing algorithms used for service interval predictions. A new crack growth measurement technique involving direct current potential difference (PD) has been developed for use in these harsh conditions. A good correlation between PD signal and crack area has been achieved. Estimations of the crack depth have been made based on fracture surface imaging, these experimentally measured crack depth propagation rates have been compared with Paris law predictions. A stress intensity factor (SIF) interaction between multiple cracks was found, where the SIF is enhanced when cracks become close. It was found that both the fatigue cycle rate and the crack shape appear to influence the SIF magnitude and the crack depth at which specimens fail, or initiate into crack propagation which is consistent with fatigue.

Introduction

Due to turbine blades being exposed to a combination of high temperatures, corrosive contaminants and cyclic loading, both accurate lifing methods and a mechanistic understanding of component degradation are required to ensure safe operation. Experimental studies have identified a corrosion cracking mechanism in superalloys under hot corrosion type conditions [1-4]. However, whilst there is a recognized mechanism in gas turbine components, increased understanding of the susceptibility of material systems to cracking and crack propagation, as well as the development of new lifing strategies are required. Therefore, experimentally measuring the crack initiation and crack growth rates (CGR) is fundamental to inform new deterministic blade lifing strategies. Linear elastic fracture mechanics (LEFM) is a commonly used methodology for the assessment of cracking and fatigue in metallic alloys [5]. Therefore the LEFM stress intensity factor (SIF) offers a useful parameter to assess cracking under combined cyclic loading and corrosion [6]. Standard approaches for experimentally measuring CGR and SIF involve testing defined geometries such as compact tension (CT) and pre-cracked type specimens [7-9]. There are several challenges with using conventional crack propagation measurement techniques in hot corrosion environments, namely:

- High temperatures and corrosive environments make the accurate use of extensometers for compliance measurements, and potential difference (PD) measurements more difficult

- The co-existing crack morphologies generated in hot corrosion environments can be complex to monitor and understand due to interactions between cracks during initiation and propagation

- Using pre-cracked or CT specimens changes the crack morphology and early crack propagation, making the crack morphologies less consistent with those observed in service components

In order to gain a better understanding of crack growth and interactions for crack initiation, corrosion cracking, and fatigue crack propagation, an experimental methodology has been developed using pulsed direct current potential difference to monitor the crack initiation and propagation rates in fatigue specimens. This study presents both cylindrical plain specimens and notched Kt specimens which were tested under combined hot corrosion and fatigue loading conditions. Previous FEA studies have found stress intensity factor interaction to be a factor when coexisting cracks become close in pipes [10-11]. In order to assess whether stress intensity factor interaction is a significant factor to consider in this work an FEA study was performed on the plain cylindrical specimen geometry. These are presented along with handbook SIF solution predictions from BS 7910 [5].

Methodology

Corrosion-Fatigue Testing with PD

The alloys of particular interest in this study are single crystal (SC) superalloys CMSX-10© and TMS-138A with nominal compositions as shown in Table 1. The specimens were longitudinally polished, cylindrical plain specimens and Kt = 1.38 notched specimens, both oriented with the <0 0 1> cube axis, aligned to the loading axis of the specimen within the tolerance of ±12°. The cylindrical gauge length of 12 mm with a 4.5 mm diameter generates a uniaxial stress state within the specimen, whilst a stress concentration factor (Kt =1.38) is present in the notched Kt specimens. Each specimen was ultrasonically cleaned in isopropyl alcohol (IPA) and sprayed with sea salt to either a known high load mass factor of 3 or a low factor of 1. The salt loading was consistent between both specimens for applied salt mass per unit area (g/m^2). These loads were chosen to represent the extremes of expected contaminant levels in service. All tests were carried out in flowing air + 300 ppm SO_x gas at 550 °C. For PD calibration purposes tests were interrupted at various times in order to produce a crack area calibration curve. Also, due to the test duration, some specimens were removed and re-salted at intervals throughout the test in order to replenish the corrosive salt species. The test conditions are summarized in Table 2.

Table 1: Nominal Compositions of CMSX-10 and TMS138A (in wt.%)

Material	Ni	Al	Cr	Co	Mo	Ti	Nb	Ta	W	Re	Ru	Hf
CMSX-10	67.8	5.9	1.7	3.1	0.5	0.1	0.1	8.5	5.5	6.8	-	-
TMS-138A	61.8	5.7	3.2	5.8	2.8	-	-	5.6	5.6	5.8	3.6	0.1

Figure 1 shows a schematic of the corrosion-fatigue (CF) test setup. Firstly, the salted specimen was loaded into the fatigue rig and then two sets of inert electrodes were spot welded onto the necked region of the specimen. The specimens are enclosed in a gastight silica glass double walled chamber with an argon shield gas. The load train passes out of either end with double seal protection to prevent process gas leakage. The chamber is then heated with an array of halogen lamps around the exterior. Cylindrical specimens were salted over the whole gauge length, whilst only one of the two notches was salted on the Kt specimens. It is critical that the location of the probes is out of the gauge so as not to generate damage from the weld that would encourage crack initiation away from the salted region of interest. The probes are then connected to a feedthrough leading out of the containment chamber and into the direct current potential difference (DCPD) system. This means that cracking can initiate anywhere along the salted gauge and thus the impact will be shown in the results. Some specimens were subject to re-salting to replenish the salts which are used up in the corrosion process. This was done by removing the specimen, re-applying the salt and then re-loading the specimen. Before re-welding the PD probes, the area of connection was lightly ground to remove oxidized material and enable a 'sound' weld. A summary of the test results presented and discussed in this paper are given in Table 2.

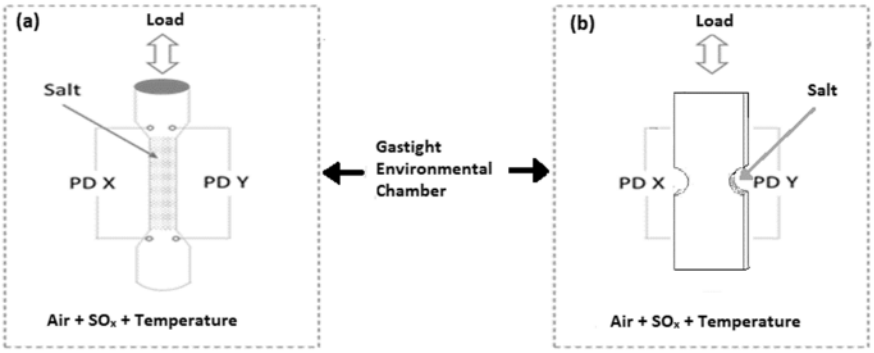

Figure 1: Schematic representation of the C-F test setup, (a) Plain cylindrical specimen salt application and attachment of probes, (b) Notched Kt specimen salt application and attachment of probes

After testing, all specimens that had not failed during the testing period were subjected to high cycle fatigue (HCF) at room temperature until the failure in order to expose the fracture surface. This enabled a clear distinction on the fracture surface between the cracking occurring at high temperature, which is monitored with PD, and that under HCF at room temperature. Each fracture surface was then examined under a 3D microscope, and the total crack area and maximum crack depths generated at high temperature under corrosion fatigue conditions were measured.

Table 2: Summary of CF test conditions

Test ID	Wave Form [s]	Salt Load factor	SO_x	Failure/ Interrupted	Temperature [°C]	Specimen Type	Peak Elastic Stress [MPa]	Material
PLAIN-1	1-1-1-1	3	Yes	Failure	550	Cylindrical	500	CMSX-10
PLAIN-2	1-1-1-1	1	Yes	Failure	550	Cylindrical	500	CMSX-10
PLAIN-3	1-60-1-1	1	Yes	Interrupted	550	Cylindrical	500	CMSX-10
PLAIN-4	1-3600-1-1	1	Yes	Interrupted	550	Cylindrical	500	CMSX-10
PLAIN-5	1-60-1-1	1	Yes	Interrupted	550	Cylindrical	500	CMSX-10
PLAIN-6	1-60-1-1	1	Yes	Interrupted	550	Cylindrical	500	CMSX-10
PLAIN-7	1-60-1-1	1	Yes	Interrupted	550	Cylindrical	500	CMSX-10
PLAIN-8	1-60-1-1	3	Yes	Interrupted	550	Cylindrical	500	CMSX-10
PLAIN-9	1-60-1-1	1	Yes	Interrupted	550	Cylindrical	500	CMSX-10
NOTCHED-1	1-120-1-1	3	Yes	Failure	550	Notched	640	TMS138A
NOTCHED-2	1-1200-1-1	3	Yes	Failure	550	Notched	640	TMS138A
NOTCHED-3	1-1200-1-1	3	Yes	Failure	550	Notched	640	TMS138A
NOTCHED-4	1-120-1-1	3	Yes	Interrupted	550	Notched	640	TMS138A
NOTCHED-5	1-120-1-1	3	Yes	Interrupted	550	Notched	640	TMS138A
NOTCHED-6	1-120-1-1	3	Yes	Interrupted	550	Notched	640	TMS138A

Evaluation of Crack Characteristics

The PD approach relies on establishing a mathematical relationship between crack area and measured PD, this relationship is nonlinear for DCPD testing. When this relationship has been established, the crack depth can be estimated from the known crack area for a given crack morphology, such as an edge crack or semi elliptical crack (Figure 2).

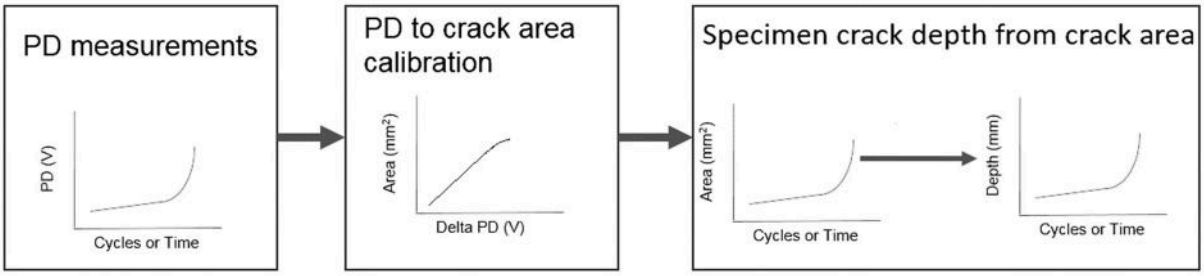

Figure 2: Outline of the method for determining crack depth from PD signal

The form of the area to PD relationship is defined as below in Equation 1, this equation has been found to represent the asymptotic relationship between resistivity and specimen area quite well.

Equation 1: Relationship between voltage and specimen area

$$\frac{V}{I} = R = \frac{\rho L}{A_{test\ piece}} = \frac{\rho L}{(A_0 - A_{crack})}$$

Where V is voltage (PD), I is current, ρ is resitivity, L is effective length between the PD probes, A_0 is the original cross sectional area of the specimen and A_{crack} is the crack area.

In order for the crack depth to then be determined from the crack area, a geometrical relationship between the two needs to be established, which is a function of the crack morphology. With cylindrical specimens, the crack morphology can vary significantly (Figure 3), with multiple initiation sites conjoining to form an effective fully circumferential crack, or initiation sites remaining isolated around the circumference of the specimen. This variability has a big influence on the prediction of crack depths and SIFs throughout the test in these cylindrical specimens.

For the notched Kt specimen geometry, it was observed that multiple cracks initiated on the salted notch. Then at some period during the test these often transitioned to an edge crack such as that presented in Figure 4 for

NOTCHED-1 and NOTCHED-3. In the NOTCHED-2 specimen the crack morphology is different from the other two, which are comparable to an edge crack.

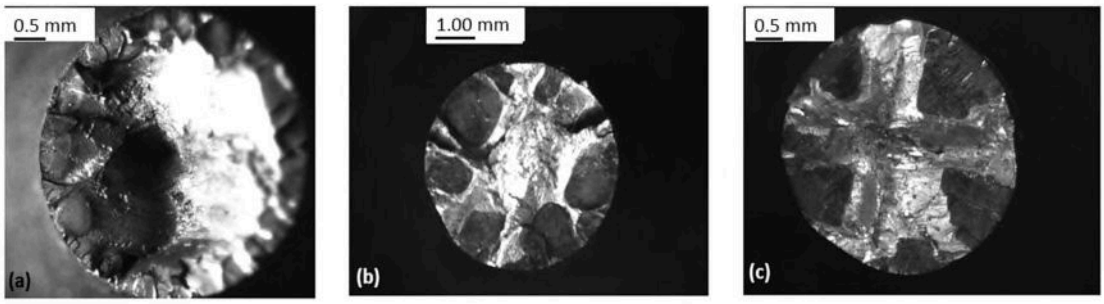

Figure 3: (a) PLAIN-2, 1-1-1-1, fully circumferential cracking (b) PLAIN-3, 1-60-1-1, isolated initiation points (c) PLAIN-4, 1-3600-1-1, isolated initiation points

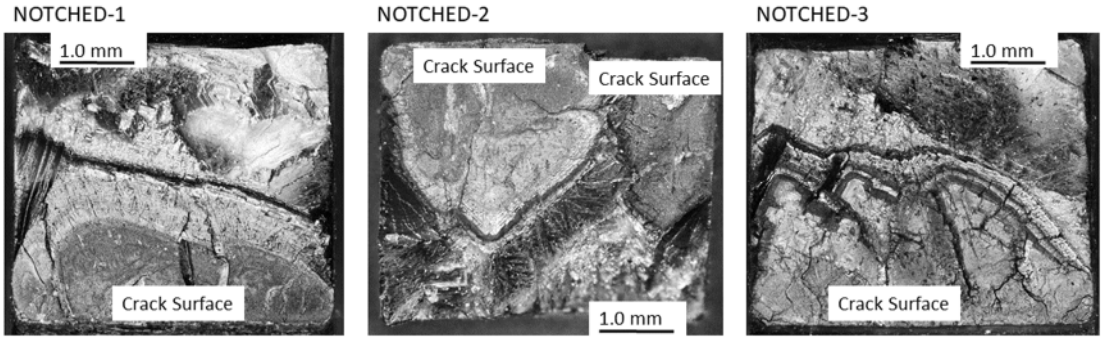

Figure 4: Notched specimen fracture surfaces

Crack SIF interaction analysis in cylindrical specimens

FE models of two semi elliptical cracks within a round bar have been built and run in ANSYS using an elastic material model and a constant load boundary condition to represent test conditions. This modelling aims to better understand the interactions of multiple flaws on the same crack plane within a cylindrical specimen, and the effects of the proximity of co-existing flaws on stress intensity. The dimensions of the models run are provided in Figure 5. The SIF factors were evaluated using the FE software's internal SIF calculation capability.

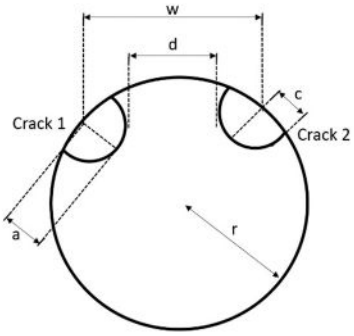

Figure 5: Multiple cracked body FE modelling parameters

A number of models were run, and are outlined in Table 3. For this initial study the two cracks had the same crack depth (a) and crack width (c) as each other, and all maintained an aspect ratio (a/c) of 1. The distance between the two cracks centres (W) remained the same for all models, meaning as the crack increased the distance between the cracks tips decreased. The specimen radius (r) remained fixed at 2.25 mm. A reference model of a single crack was also run in order to calculate the interaction factor, for each crack size.

The SIF interaction models were meshed and run in ANSYS, assuming geometric linearity, with a unit isotropic elastic stiffness. A pressure load boundary was used to represent the load control test conditions, mesh examples are given in Figure 6 and Figure 7.

Table 3: Multiple cracked body models matrix, total of 14 models

	2 Cracks	**1 Crack**
a/r	**d (mm)**	**d (mm)**
0.1	2.8	2.8
0.4	1.45	1.45
0.45	1.225	1.225
0.5	1	1
0.55	0.775	0.775
0.6	0.55	0.55
0.63	0.41	0.41

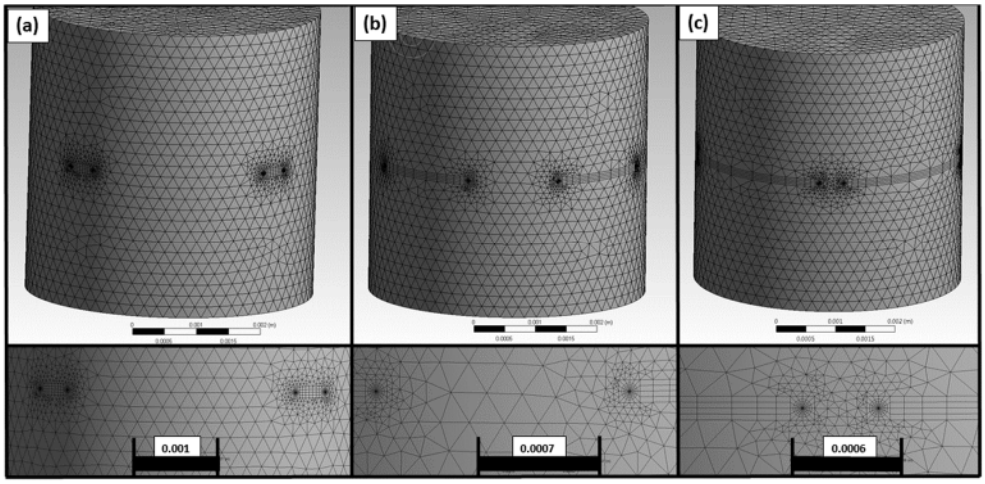

Figure 6: Mesh images of multiple cracked body FE models; (a) a/r = 0.1; (b) a/r = 0.4 (c); a/r = 0.63

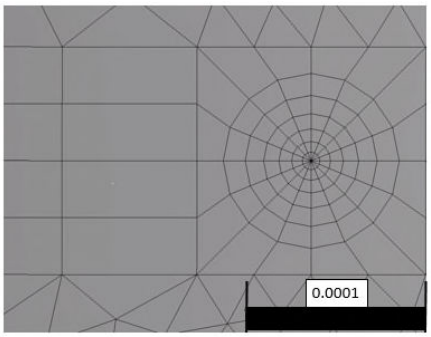

Figure 7: Focused crack tip mesh of cracked body FE models

The interaction between the two cracks was calculated as shown in Equation 2 using SIF geometry factors normalised against the geometry factor for a single crack.

Equation 2: Crack interaction factor calculation

$$\gamma = \frac{Y_{2\ cracks\ conjoining\ side}}{Y_{1\ single\ crack}}$$

SIF Prediction for notched specimens using handbook solutions from BS 7910

The SIFs were predicted for notched specimens at the point of failure using a handbook solution for edge cracks from BS 7910 section Q.7. [5]. This approach assumes an infinite width plate, or plane strain conditions. The approach accounts for the stress profile across the depth of a double notched specimen as a polynomial function which was calculated using an FE model. For the NOTCHED-2 specimen the crack geometry does not closely represent a 1D edge crack and the BS 7910 handbook solution is not valid for this specimen.

Results and Discussion

Crack Area Calibration

For the plain cylindrical specimens, the measured crack area vs measured PD are presented in Figure 8 where the predicted line is the fitted form of Equation 1 rearranged for crack area, and where ρL is the fitted parameter. It can be observed that the trend is close to linear for the plain cylindrical specimens, due to the small crack area compared with the cross sectional area of the specimen (Figure 3). This combined with the scatter observed in these specimens' means, a linear simplification is a suitable assumption to estimate the crack area to PD relationship for this specimen geometry. Due to the large variation in crack morphologies present in the plain cylindrical specimens, accurate prediction of crack depth propagation from the crack area is difficult.

The measured crack areas for the notched specimens are plotted against the final PD in Figure 8, where the predicted line is the fitted form of Equation 1. It can be observed that this specimen geometry exhibits more non-linearity in its calibration response and therefore the calibration form given in Equation 1 provides a good representation of the behavior. The notched specimens also transition to an edge type crack relatively early on in the tests, and as such a good prediction of the crack depth propagation can be made.

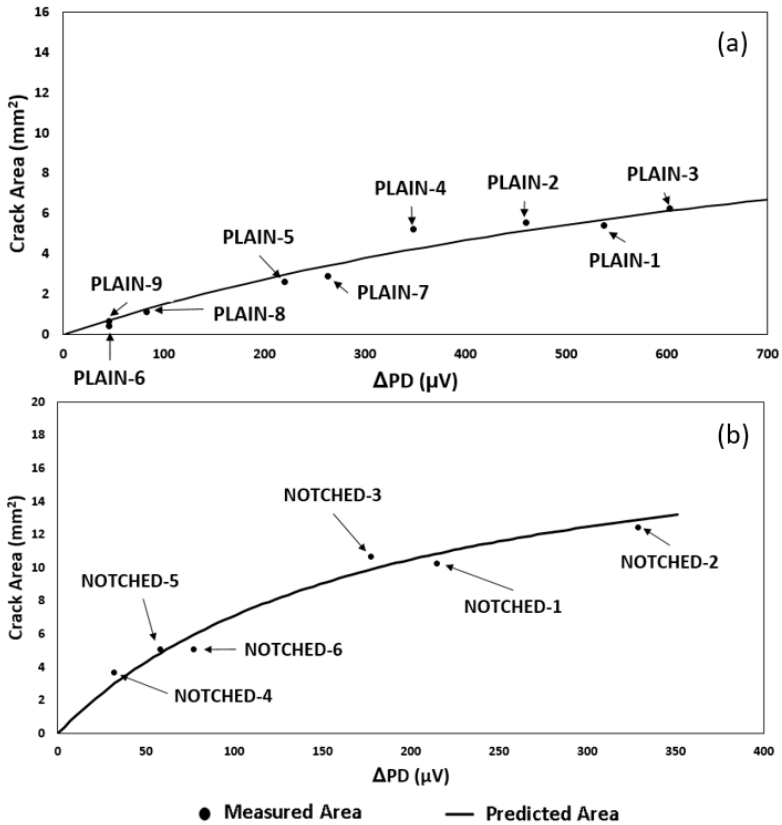

Figure 8: (a) Plain specimen's area calibration, (b) Notched specimen's area calibration

Crack Propagation Test Results

Plots of crack area against cycles and time for all the plain cylindrical specimens are presented in Figure 9 using the linear calibration simplification previously discussed. The following observations can be made from the cylindrical specimen results:

- The longer 3600 s dwell PLAIN-3 specimen propagated to a larger crack area than the two failed 1 s dwell specimens (PLAIN-1 and PLAIN-2).

- The 3600 s dwell test exhibited a relatively constant and time dependent rate of propagation, where a resalting at 100 cycles initiated a more rapid rate of propagation.

- The two 1 s dwell tests reach a crack size after which the propagation behavior changes, this occurs after a resalt at 60,000 cycles.

- The final part of the propagation curve on the two 1 s dwell tests is more in line with Paris mechanical fatigue behavior, where the rate of propagation increases as the crack grows.

- The initial period of crack growth in the PLAIN-1 specimen is greater than that measured in the PLAIN-2 specimen. These specimens test conditions were identical, other than PLAIN-1 was subject to the high salt load factor of 3 and PLAIN-2 was subjected to the low salt load factor of 1.

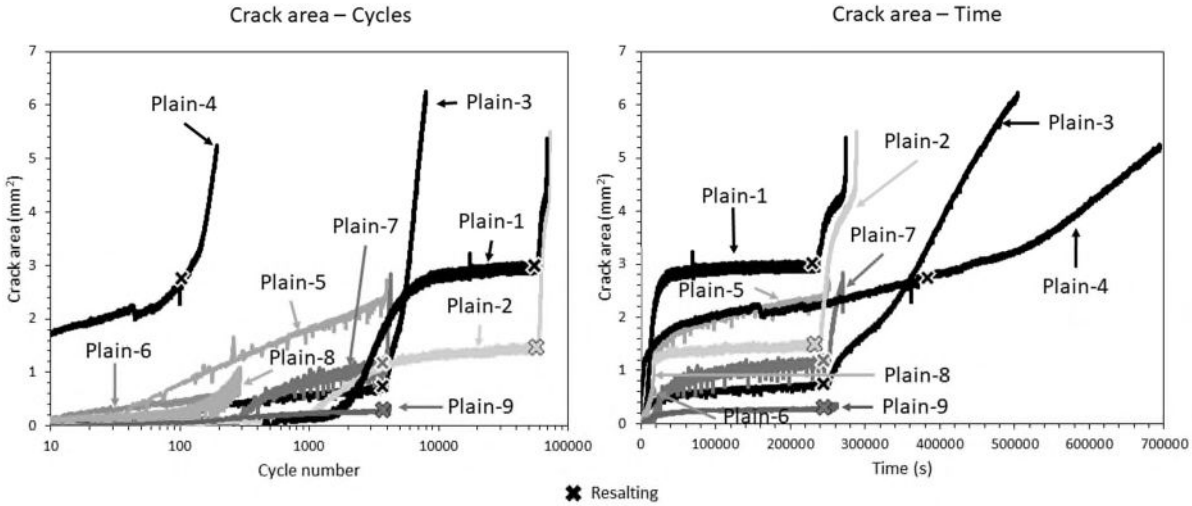

Figure 9: Crack area plots for plain cylindrical tests using linear calibration simplification

Plots of crack depth against cycles and time for the three failed notched specimens are presented in Figure 10, these are generated from the non-linear calibration, assuming an edge crack morphology. This means that the crack depths are likely be under-predicted at the start of the test when the cracks are likely to be of a semi-elliptical morphology. There is a strong correlation between resalting, and a subsequent period of increased crack propagation rate in the PD trace. This increased rate then tails off into a period of constant propagation. These resalting induced jumps in crack growth are more visible earlier on in the test of the three specimens presented below.

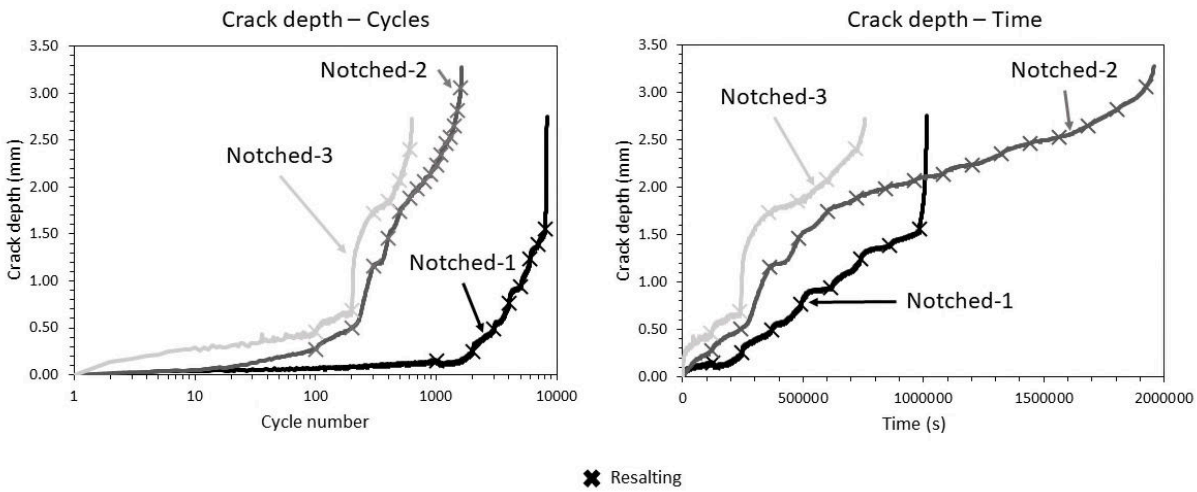

Figure 10: Notched crack depth propagation curves for failed specimens

SIF Interactions

FE results for the far edge (side of the crack furthest from the second crack), near edge (side of the crack nearest the second crack) and a single crack are presented in Table 4, where (r) is the specimen radius and (d) is the distance between the closest points of the crack tips (Figure 5). A good indicator of the accuracy and suitability of the mesh of a cracked-body FE models is the convergence of the calculated SIFs for each resolved contour region. The SIFs presented were extracted from the outer most contour region, however the outer four contour regions had all converged well. The interaction between the cracks was calculated as defined in Equation 2. This is plotted against the angle around the crack tip for various d/r ratios and is presented in Figure 11.

Table 4: geometry factors from FE and BS 7910 (Y)

Surface						
a/r	**a/d**	**d (mm)**	**d/r**	**2 Cracks Far Edge (Y)**	**2 Cracks Near Edge (Y)**	**1 Crack Surface (Y)**
0.1	0.080	2.8	1.244	0.6849	0.6831	0.6832
0.4	0.621	1.45	0.644	0.7879	0.8177	0.8008
0.45	0.827	1.225	0.544	0.8151	0.8697	0.8300
0.5	1.125	1	0.444	0.8500	0.9480	0.8667
0.55	1.597	0.775	0.344	0.8913	1.0572	0.9100
0.6	2.455	0.55	0.244	0.9485	1.2613	0.9605
0.63	3.459	0.41	0.182	0.9940	1.5155	0.9962
Deepest Point						
a/r	**a/d**	**d (mm)**	**d/r**	**2 Cracks Deepest Point (Y)**		**1 Crack Deepest Point (Y)**
0.1	0.080	2.8	1.244	0.6442		0.6461
0.4	0.621	1.45	0.644	0.7322		0.7246
0.45	0.827	1.225	0.544	0.7644		0.7473
0.5	1.125	1	0.444	0.8013		0.7735
0.55	1.597	0.775	0.344	0.8555		0.8047
0.6	2.455	0.55	0.244	0.9302		0.8323
0.63	3.459	0.41	0.182	1.0019		0.8558

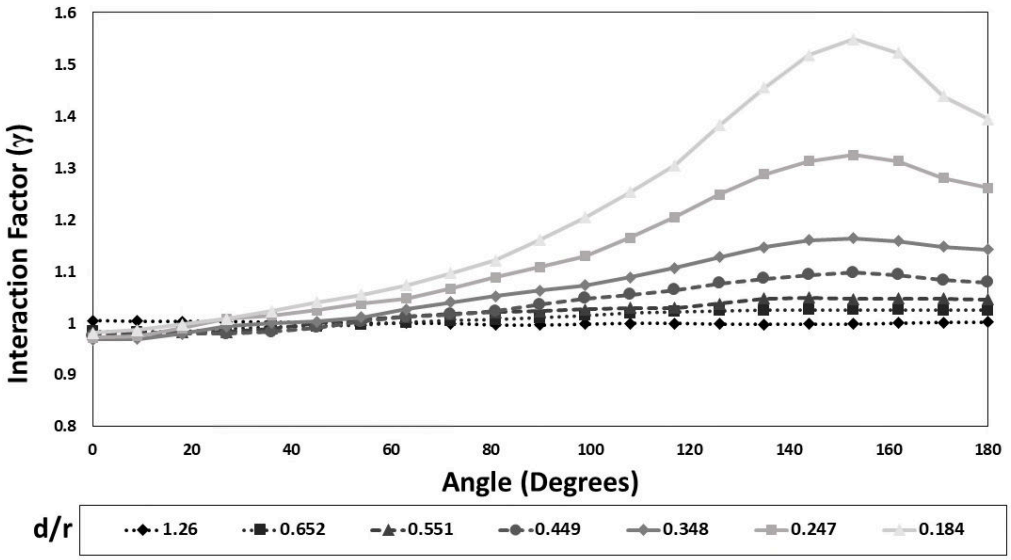

Figure 11: FE predicted SIF interaction between two cracks in cylindrical specimen

There is a SIF interaction effect captured in the FE study, where the SIF is increased when two co-existing cracks propagate to within close proximity of one another. A maximum factor of 1.55 times the SIF geometry factor was calculated for cracks which were 0.41 mm apart. However, this trend would presumably continue to increase as the cracks propagate to within closer proximity to one another. Until the crack depth (a) becomes similar to the distance between the cracks (d), the interaction effect is relatively small. The SIF interaction study demonstrates the complications of accurately interpreting crack growth and SIF in the cylindrical specimen geometry.

Crack propagation rates and SIF predictions for notched specimens

The crack propagation rates for notched specimens were calculated from the crack depth against cycles data presented in Figure 10. This data has been combined with the SIF predictions which were calculated using the handbook SIF solution for an edge crack from BS 7910, to give a Paris type plot presented in Figure 12. The SIF predictions were calculated for the final fracture surface and the geometry factor was assumed as the constant for plotting the Paris curves in Figure 12. For the NOTCHED-2 specimen a SIF solution could not be calculated due to the final fracture surface not representing an edge crack. For this specimen, the SIF was assumed to be the same as NOTCHED-3, which was tested under the same conditions.

It can be seen that at the end of the test, the crack propagation curve starts to conform to the exponential Paris law, forming a relatively straight line on a log-log plot, this behavior can be observed in all three specimens presented. Before this exponential behavior is observed, there is still a significant rate of crack propagation

occurring, however shows little correlation to ΔK and more to resalt and corrosive factors, suggesting that the early crack growth is more a function of the corrosive environment.

The point at which the crack propagation switches to conform to the exponential Paris crack growth law can be considered a threshold referred to here as the pure fatigue threshold. In the results presented in Figure 12, it is observed that the dwell time influences the SIF at which this pure fatigue threshold occurs. Vertical lines signifying the region where this threshold occurs have been visually placed on the graph to highlight this trend.

The pure fatigue threshold for the faster fatigue cycle with a smaller 120 s dwell time, occurs at a lower SIF than the longer 1200 s dwell time. Additionally the subsequent Paris curve which takes effect at SIFs higher than the threshold, sits at a higher rate of propagation (da/dN) for the 120 s dwell than it does for the longer 1200 s dwell curves. As there is an increased amount of corrosion accrued per cycle in the longer dwell tests, these observations support a hypothesis of corrosion suppressing the SIF at which the pure fatigue threshold is overcome, and slowing the subsequent cycle dependent crack propagation rate. This could be the result of corrosion dependent phenomena such as crack closure reducing the effective ΔK [12] or crack tip blunting where similar effects have been observed in SC superalloys between air and vacuum tests [13].

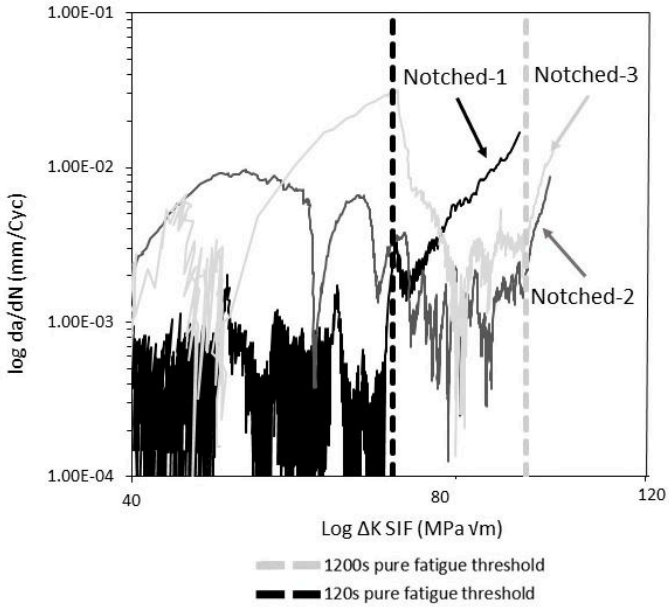

Figure 12: Paris curve for three failed notched specimens, where the threshold lines have been placed by eye

Conclusions

Both the plain cylindrical specimens and the notched Kt specimens tested follow the non-linear PD to crack area calibration relationship. This calibrated PD technique offers a good approach to measure crack area propagation in high temperature corrosion environments. Determining the change in crack depth throughout the tests for cylindrical specimens was difficult due to the variability in crack morphologies present. As such, cylindrical specimens were good for recreating multiple crack initiation features and corrosion driven crack growth, but were not best suited for detailed crack propagation measurement. However, for notched specimens the PD methodology offers good predictions for crack depth and propagation rates using the edge crack morphology. Therefore, this specimen geometry was better suited for more detailed crack propagation analysis. Further testing exploring the crossover from semi-elliptical to edge crack would help to understand and better predict short crack growth using the PD methodology.

Increasing corrosion per cycle through increased dwell time and salt load lead to accelerated or increased rates of early corrosion driven crack propagation. However, it was observed in the three notched specimens analyzed, that corrosion did influence the fatigue propagation, by increasing the crack size and predicted SIF at which propagation became consistent with Paris law, and reducing the subsequent rate of fatigue crack propagation. This suggests a mechanism of corrosion suppressing cycle dependent crack propagation or fatigue. Ultimately, however, the corrosion mechanism studied dominated both the crack initiation, and the shorter crack propagation and as such had a net negative impact on the overall specimen life.

FE studies were performed in order to predict the SIF interactions between co-existing cracks within close proximity to one another in cylindrical specimens. It was found that there was a notable SIF interaction effect, where a factor of 1.55 times the SIF was found for given crack aspects. This interaction between cracks could therefore be an important consideration when interpreting and analyzing detailed fatigue crack growth of co-existing cracks in cylindrical specimens.

Acknowledgments

This work has been funded by Innovate UK ATI under the MALIT program (Grant no. 103081-263288) and EPSRC Platform Grant in 'Through Life Performance: From Science to Instrumentation'.

References

[1] Brooking L, Sumner J, Gray S, Nicholls JR, Marchant G, Simms NJ (2018) Effect of stress state and simultaneous hot corrosion on the crack propagation and fatigue life of single crystal superalloy CMSX-4. Int. J. Fatigue 116:106-117. doi:10.1016/j.ijfatigue.2018.05.002

[2] Brooking L, Gray S, Dawson K, Nicholls JR, Simms NJ, Sumner J, Tatlock GJ (2020) Analysis of combined static load and low temperature hot corrosion induced cracking in CMSX-4 at 550°C. Corros. Sci. 163. doi:10.1016/j.corsci.2019.108293

[3] Cockings HL, Perkins KM, Dowd M (2017) Influence of environmental factors on the corrosion-fatigue response of a nickel-based superalloy. Mater. Sci. Technol. 33(9):1048-1055. doi:10.1080/02670836.2017.1300419

[4] Pedrazzini S, Child DJ, Aarholt T, Ball C, Dowd M, Girling A, Cockings H, Perkins K, Hardy MC, Stone HJ, Bagot PAJ (2018) On the effect of environmental exposure on dwell fatigue performance of a fine-grained nickel-based superalloy. Met. and Mat. Trans. A 49:3908-3922. doi:10.1007/s11661-018-4752-7

[5] British Standards Institution (2013) Guide to methods for assessing the acceptability of flaws in metallic structures. BS7910:2013+A1:2015

[6] Chan KS, Enright MP, Moody JP (2014) Development of a probabilistic methodology for predicting hot corrosion fatigue crack growth life of gas turbine engine disks. J. Eng. Gas Turbines Power 136(2):022505. doi:10.1115/1.4025555

[7] ASTM International (2015) Standard test method for measurement of fatigue crack growth rates. ASTM E647-15e1

[8] ASTM International (2020) Standard test method for linear-elastic plane-strain fracture toughness of metallic materials. ASTM E399-20

[9] Zhu XK, Joyce JA (2012) Review of fracture toughness (G, K, J, CTOD, CTOA) testing and standardization. Eng. Fract. Mech. 85:1-46. doi:10.1016/j.engfracmech.2012.02.001

[10] Coules HE (2018) On predicting the interaction of crack-like defects in ductile fracture. Int. J. Press. Vessel. Pip. 162:98-101. doi:10.1016/j.ijpvp.2018.03.006

[11] Coules HE (2016) Stress intensity interaction between dissimilar semi-elliptical surface cracks. Int. J. Press. Vessel. Pip. 146:55-64. doi:10.1016/j.ijpvp.2016.07.011

[12] Brown CW, Hicks MA (1982) Fatigue growth of surface cracks in nickel-based superalloys. Int. J. Fatigue 4(2):73-81. doi:10.1016/0142-1123(82)90063-9

[13] Joyce MR, Wu X, Reed PAS (2004) The effect of environment and orientation on fatigue crack growth behaviour of CMSX-4 nickel base single crystal at 650°C. Materials Letters 58(1-2):99-103. Doi:10.1016/S0167-577X(03)00423-3

Measurement and evaluation of co-existing crack propagation in single-crystal superalloys in hot corrosion fatigue environments

Brooking, L.

2021-08-29

Brooking L, Ferguson C, Mason-Flucke J, et al., (2020) Measurement and evaluation of co-existing crack propagation in single-crystal superalloys in hot corrosion fatigue environments. In: 14th International Symposium on Superalloys (Superalloys 2020), Seven Springs Pa, USA
https://doi.org/10.1007/978-3-030-51834-9_75